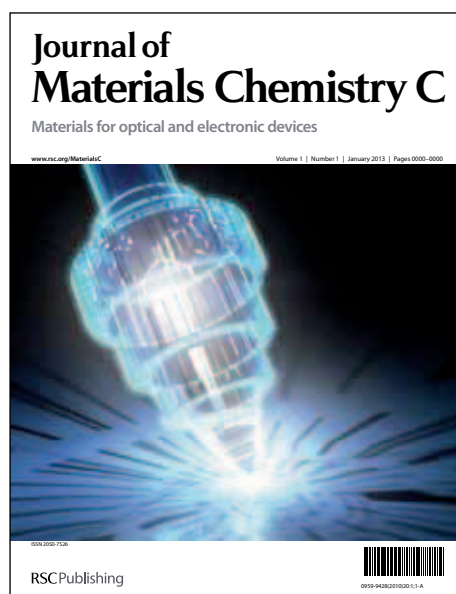


Journal of Materials Chemistry C

Accepted Manuscript



This is an *Accepted Manuscript*, which has been through the RSC Publishing peer review process and has been accepted for publication.

Accepted Manuscripts are published online shortly after acceptance, which is prior to technical editing, formatting and proof reading. This free service from RSC Publishing allows authors to make their results available to the community, in citable form, before publication of the edited article. This *Accepted Manuscript* will be replaced by the edited and formatted *Advance Article* as soon as this is available.

To cite this manuscript please use its permanent Digital Object Identifier (DOI®), which is identical for all formats of publication.

More information about *Accepted Manuscripts* can be found in the [Information for Authors](#).

Please note that technical editing may introduce minor changes to the text and/or graphics contained in the manuscript submitted by the author(s) which may alter content, and that the standard [Terms & Conditions](#) and the [ethical guidelines](#) that apply to the journal are still applicable. In no event shall the RSC be held responsible for any errors or omissions in these *Accepted Manuscript* manuscripts or any consequences arising from the use of any information contained in them.

ARTICLE

Structural Feature and Optical Property of a Carbazole-Containing Ethene as Highly Emissive Organic Solid

Cite this: DOI: 10.1039/x0xx00000x

Received 00th January 2012,
Accepted 00th January 2012

DOI: 10.1039/x0xx00000x

www.rsc.org/

Yang Liu,^{*a} Xin Ye,^a Guangfeng Liu,^a Yun Lv,^a Xiying Zhang,^a Shuming Chen,^c Jacky W. Y. Lam,^b Hoi Sing Kwok,^c Xutang Tao^{*a} and Ben Zhong Tang^{*bde}

Carbazole derivatives are a kind of versatile materials especially for optoelectronic applications in light of their activity in both electronics and optics. To suppress the luminescence quenching effect in the condensed phase, we constructed a carbazole derivative with aggregation-induced emission characteristic. The highly emissive organic solid of carbazole-substituted ethane was facilely prepared and thoroughly tested. Through inspection of the geometric structure and packing motifs of the crystalline materials, the severe twisted conformation and the absence of strong intermolecular π - π interactions are found to account for the extreme solid state quantum yield. The highly blue emissive crystal fibres exhibit optical waveguide property. Electroluminescence (EL) study reveals the hole-transporting nature of the material.

Introduction

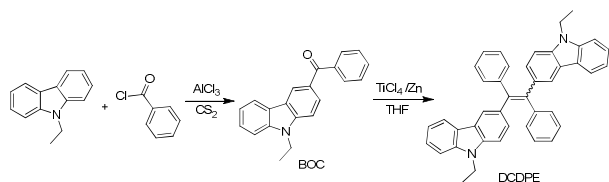
Carbazole is a nitrogen-bridged biphenyl isoelectronic to fluorene. Oligomers and polymers based on carbazole have been widely investigated as materials for optoelectronic applications such as xerography, organic transistors, organic light-emitting diodes (OLEDs) and photovoltaic devices.¹ They possess higher HOMO energy levels than that of fluorenes, which is favourable of hole transporting abilities.² A number of carbazole derivatives have been designed and synthesized for hole-transporting layers and host materials for red, green and even blue triplet emitters.³ However, the carbazole derivatives themselves used as light-emitting materials have been suppressed by the aggregation-caused quenching (ACQ) effect.^{4,5} This problem is also identified as a major concern for most of the common organic chromophores.⁶ From a chemical standpoint, the problem can be solved or alleviated by designing sterically hindered compounds.⁷ However, because the luminophores have an inherent tendency to aggregate in the condensed phase, the approaches are basically working against a very natural process and have thus ended up with only limited success and partial control. In a sharp contrast, using the idea of aggregation-induced emission (AIE), the intrinsic aggregation is no longer a suffering process.⁸ Oppositely it takes advantage

of the aggregation process, and thus does not have any issues of temporal or spatial instabilities. We have explored high-tech applications of the AIE luminogens as, for example, fluorescence sensors (for explosive, ion, pH, temperature, viscosity, pressure, *etc.*), biological probes, and active layers in the OLEDs.⁹

Although luminogens with AIE characteristic are no longer novel stuffs after years of massive research, the development of more fantastic and practical ones suitable for different applications is significant. This indeed depends on the fully understanding of the mechanism and the structure particularity of the discovered ones. Analysing the structure and packing characteristics of them will help us to deepen the understanding and further facilitate the design of new highly emissive organic solids. In this report, we have successfully designed and synthesized a carbazole-containing tetrasubstituted ethene through a facile strategy. It showed typical AIE property and extremely high solid-state fluorescence efficiency. By digging into its structure feature, the propeller molecular geometry-caused loose packing was considered to respond for the highly luminescent ability in the solid state. Such a strategy is universal for most of the chromophores those originally being ACQ to become AIE.

Results and Discussions

Synthesis



Scheme 1 Synthetic route to 1,2-bis(N-ethyl-3-carbazole)-1,2-diphenylethylene (DCDPE).

Scheme 1 shows the chemical structure and synthetic route of the carbazole-containing AIE lumigen 1,2-bis(N-ethyl-3-carbazole)-1,2-diphenylethylene (DCDPE). Firstly, carbazole was incorporated into the ketone intermediate 9-ethyl-3-benzoylcarbazole by an AlCl_3 catalysed Friedel-Crafts acylation.¹⁰ Then the Zn/TiCl_4 catalysed McMurry coupling reaction produced the target in a high yield.¹¹ Details of the synthetic procedures and characterization data are presented in the Supporting Information. The dye molecule was characterized by NMR spectroscopy and gave high signal: noise ^1H and ^{13}C NMR spectra. The reaction product gave M+ peaks at their high-resolution mass spectra, confirming the occurrence of the coupling reaction and the formation of the expected product. The purity of the product was also confirmed by elemental analysis with satisfactory result. McMurry coupling of BOC results in two different isomers with a ratio of about 1:1 calculated from the ^1H NMR spectra. We obtained pure *trans*-isomer by recrystallization of the pre-purified product via column chromatography in DCM/ethanol mixture. In the later experiments of thermal and electrochemical properties and EL performance tests, we used *trans*-form of DCDPE.

Optical properties

DCDPE is soluble in common organic solvents such as chloroform and THF but insoluble in water. It is practically nonemissive when molecularly dissolved in the solutions. As shown in Figure 1, the PL spectrum of DCDPE in THF is basically a flat line parallel to the abscissa. The fluorescence quantum yield in THF is as low as 0.22%, revealing that DCDPE is genuinely weak emitters as the free isolated molecular species. When a large amount of water is added into its THF solution, intense PL signals are recorded at 502 nm under the identical measurement conditions. The emission intensity starts to rise when the water fraction is larger than 75%, where the solvating power of the mixture is worsened to such an extent that the luminogen molecules begin to aggregate. From the molecular solution in THF to the aggregate suspension in 95% aqueous mixture, the fluorescence intensity increases ca. 412-fold and the fluorescence quantum yield value increases ca. 182-fold. The photograph given in the inset of Figure 1B clearly shows the changing from the nonemissive to emissive nature of the molecular species and the aggregative particles of DCDPE. Apparently, its emission is induced by aggregate formation. The aqueous mixtures are, however, macroscopically homogenous with no precipitates, suggesting that the aggregates are of nanodimension, as proved by the example of transmission electron microscope (TEM) images shown in Figure S6 and the level-off tails at the long wavelength region of their absorption spectra in the aqueous mixtures with high water contents due to the scattering effect of the dye nanoparticles (Figure S5).¹² The measurement of the fluorescence quantum yields of DCDPE in the real solid state further validates its AIE activity, which is as high as 99% in the solid thin film determined by integrating sphere.

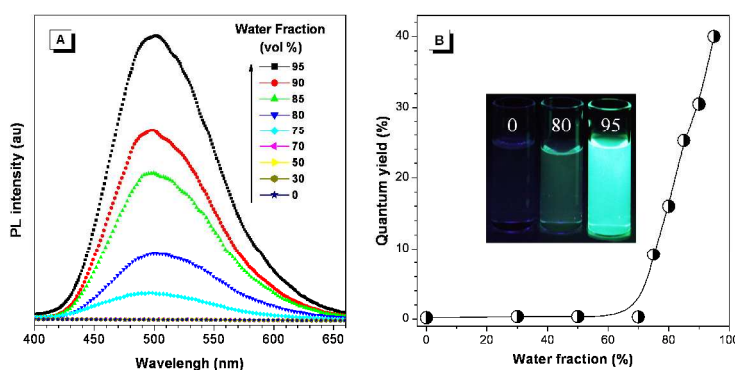


Fig. 1 (A) Photoluminescence spectra of DCDPE in THF/water mixtures with different water fractions. Concentration: 10 μM ; excitation: 355 nm. (B) Plots of fluorescence quantum yields versus compositions of the THF/water mixtures. Inset: Fluorescent photos of DCDPE in THF/water mixtures with 0%, 80% and 95% water fractions.

Structural analysis

In an effort to understand the mechanism operating in the AIE system, we checked the geometric structure and packing motifs of DCDPE in the crystalline state. The molecules crystallize easily from the mixture solvent of dichloromethane and ethanol.

Figure 2 shows the X-ray determined molecular structure. The molecule adopts a quite twisted conformation, with the four substituted aromatic rings arranged in a propeller-like shape along the ethene. The dihedral angles between each two aromatic planes of DCDPE are listed in Table 1, which are in the range from 54.5° to 83.3°. For example, the two phenyl

rings (represented by Cg(5) and Cg(8)) make a dihedral angle of 83.3° ; while the two carbazole rings (represented by Cg(13) and Cg(14), not listed in Figure 2) are with a dihedral angle of 62.5° . The quite severe intramolecular torsion indicates such non-coplanar propeller-shaped structure will prevent the luminogens from packing in a close π - π stacking mode. This is

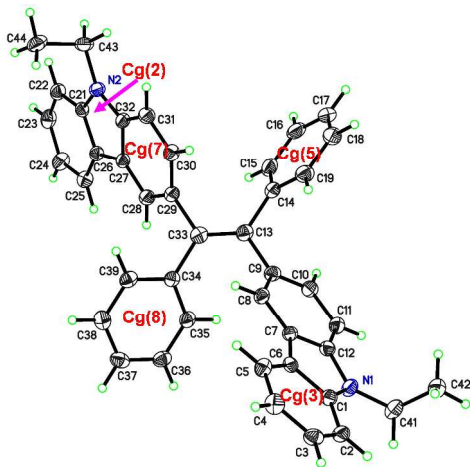


Fig. 2 Molecular structure of DCDPE obtained by X-ray diffraction. Cg(i) stands for aromatic planes (π rings).

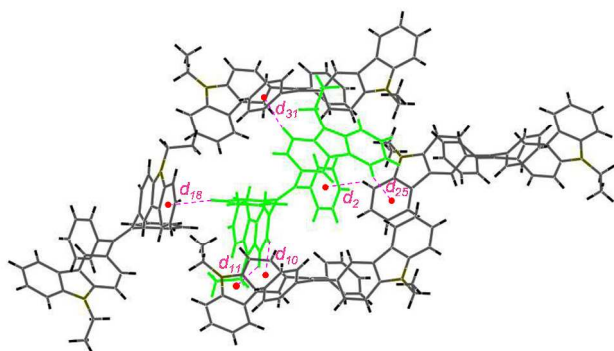


Fig. 3 Packing arrangement in the crystal structure of DCDPE, with C-H $\cdots\pi$ hydrogen bonds marked by dashed lines. dx stands for the distance between the H atom of C(x)-H(xA) to plane Cg(j).

proven by the packing motif of DCDPE in crystals. As can be seen from Figure 3, the intermolecular π - π interactions and other strong intermolecular interactions are totally absent. At the same time, the intramolecular bond rotational and vibrational freedom is still restricted by the intermolecular C-H $\cdots\pi$ hydrogen bonds formed between the aromatic hydrogens and the aromatic rings. From figure 3 we can see one DCDPE molecule forms six C-H $\cdots\pi$ hydrogen bonds with four of its neighbour molecules. Table 1 lists all the parameters of the intermolecular C-H $\cdots\pi$ hydrogen bonds. The distances range from 2.75 Å to 2.86 Å and the angles (γ) of C(x)-H(xA) to Cg(j) (vector and normal to plane Cg(j)) range from 8.06° to 15.77° , within the standards of C-H $\cdots\pi$ interactions of 3.0 Å and 30° .¹³ These kinds of weak interactions rigidify the molecular conformation and lock the vibrational freedom of the

chromophores, but do not afford any energy decay channels such as the π - π interactions or excimer formation. The weak intermolecular interactions plus the severe twisted intramolecular geometry are the factors account for the extremely high quantum yield of DCDPE solids. Figure 4 shows the fluorescent microscopic images of the crystalline clusters of DCDPE under UV excitation. The crystalline samples are highly luminescent, emitting intense blue light upon photoexcitation. Glaring light emissions are seen at the ends of the microfibers indicating that an optical waveguide effect is operating in the light transmission process of the microfibers. The waveguide effect is usually observed in an optically anisotropic system, such as crystalline assembly. The crystallinity has significant effect on the emission behavior of DCDPE, which results in its fluorescence wavelength shifting from 483 nm in crystalline to 511 nm in amorphous, as shown in Figure S7. The fluorescence quantum yields in both states are as high as 99%, while in crystalline fibers it seems brighter due to the light scattering of the crystal facets. Such kind of efficient luminescent crystals are desired for light-emitting and laser applications.

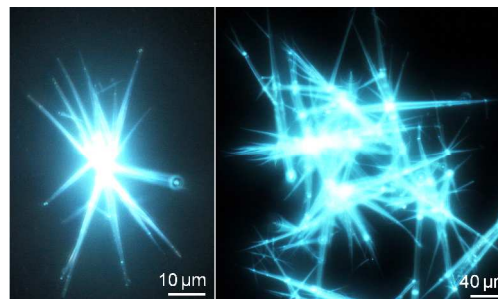


Fig. 4 Fluorescence microscopic images of crystalline clusters of DCDPE with different scales.

Thermal and Electrochemical properties

The thermal properties of DCDPE are investigated by the Thermogravimetric Analysis (TGA) and Differential Scanning Calorimetry (DSC). The dye is thermally stable up to 380 °C (T_d , the decomposition temperature) as determined by the TGA measurement shown in the inset of Figure 5. DSC scan result represented in Figure 5 shows that the initial crystalline sample melted at 252 °C to give an isotropic liquid in the first run of the DSC measurement. Upon cooling, the isotropic liquid changed into a glassy (amorphous) state. As the glassy sample was reheated for the second run, a glass transition was observed at 119 °C, which is defined as the glass transition temperature (T_g) of DCDPE. Thus although the molecular weight of DCDPE is not so high, its T_g is much higher than that of the commonly used hole-transporting material (e.g., 98 °C for NPB),¹⁴ which may be attributed to the rigid structure. (The T_m of NPB is $\sim 280^\circ\text{C}$ and T_d is 370 °C) The high morphological stability coupled with the efficient solid-state emission render the dye a promising EL material. It is well known that carbazole derivatives usually possess higher HOMO energy levels and good charge transport abilities. Thus to determine its

energy level, the electrochemical property of DCDPE was studied by the cyclic voltammetry. The electrochemical potential was calibrated with the ferrocene/ferrocenium (Fc/Fc⁺) standard (4.8 eV below the vacuum level). As shown in Figure 6, the compound shows a reversible oxidation process in CH₃CN solution. The oxidation peak occurs at 0.50 V. From the onset of the oxidation, its HOMO energy level is estimated at 5.2 eV, slightly higher than that of NPB. The LUMO energy level of DCDPE deduced from the difference between the HOMO level and the optical band gap is 2.1 eV. As shown in Figure 7, comparing with NPB, it possesses higher-lying

LUMO level, which is beneficial to blocking of electron leakage to the anode. On the other hand, its higher HOMO level is more close to the work function of the ITO anode, which can lower the charge injection barrier and the device operating voltages. These electronic properties indicate that besides light-emitting, DCDPE can also play a role as hole-transporting material. Thus according to the energy level diagrams, two different device architectures are adopted to validate its optoelectronic property. One is the typical device structure with both hole-transporting and electron-transporting layers (HTL & ETL) and the other one is only with of ETL (Figure 7).

Table 1 Analysis of dihedral angles between intramolecular aromatic planes (π rings) and C-H... π intermolecular interactions in the crystal packing of DCDPE.

Planes (Cg(i), Cg(j)) ^a	Angles ($^{\circ}$)	Atoms to planes (C(x)–H(xA) \rightarrow Cg(j)) ^a	Distances (\AA)	γ^b ($^{\circ}$)
Cg(5), Cg(8)	83.3	d_2 C(2)–H(2A) \rightarrow Cg(8)	2.81	8.06
Cg(5), Cg(13)	83.2	d_{10} C(10)–H(10A) \rightarrow Cg(7)	2.75	11.78
Cg(5), Cg(14)	54.5	d_{11} C(11)–H(11A) \rightarrow Cg(2)	2.86	13.63
Cg(8), Cg(13)	57.7	d_{18} C(18)–H(18A) \rightarrow Cg(3)	2.86	14.12
Cg(8), Cg(14)	81.8	d_{25} C(25)–H(25A) \rightarrow Cg(3)	2.77	6.00
Cg(13), Cg(14)	62.5	d_{31} C(31)–H(31A) \rightarrow Cg(5)	2.85	15.77

^a Planes number of Cg(i), Cg(j) and atom number are from Figure 2; Cg(13) and Cg(14) stands for the two carbazole planes. ^b γ is the angle of C(x)–H(xA) to Cg(j) vector and normal to plane Cg(j).

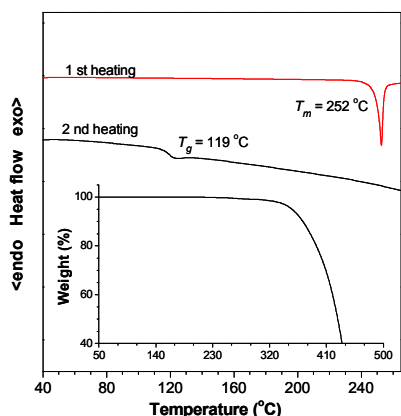


Fig. 5 DSC thermograms of DCDPE recorded under N₂ at a heating rate of 10 °C/min. Inset: TGA thermogram of DCDPE.

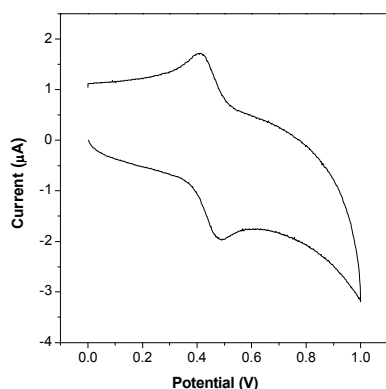


Fig. 6 Cyclic voltammograms of DCDPE in 0.1 M Bu₄NPF₆/CH₃CN.

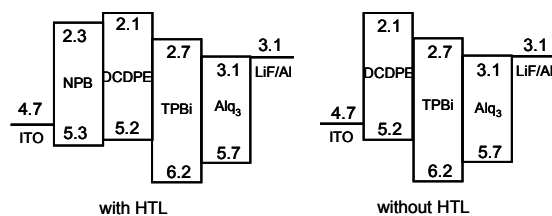


Fig. 7 Energy level diagrams and device configurations of multilayer EL devices of DCDPE.

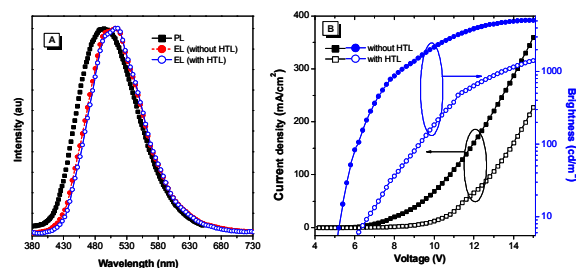


Fig. 8 (A) PL and EL spectra of DCDPE. (B) Current density and luminance versus voltage characteristics of devices based on DCDPE.

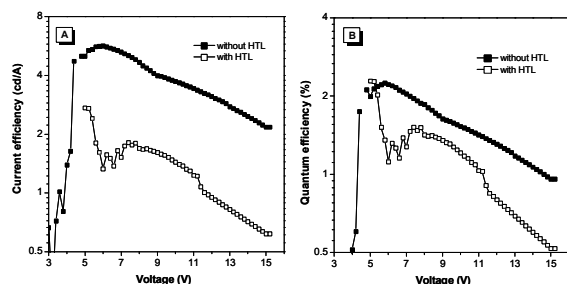


Fig. 9 (A) Current efficiency and (B) External quantum efficiency (%) versus voltage characteristics of devices based on DCDPE.

Electroluminescence properties

For the typical device structure with both HTL and ETL, the device emits bluish green light with an EL maximum (λ_{EL}) of 512 nm, which is close to that of the PL in thin film. For the simple device structure without dedicated HTL, the device emits at almost the same wavelength, revealing no migration of the emitting region. Figure 8A depicts the EL and PL spectra. In both devices the EL show spectra stability with hardly changes along with the operating bias increasing from 8 V to 15 V. Figure 8B shows the current density and luminance versus voltage characteristics of the two kinds of devices. We can see that with the simple configuration (no dedicated HTL), the device shows much better electronic character. To reach a same current density/brightness, the applied bias needed for the latter device is much higher than that for the simple one. That means the charge transfer in the simple device is more efficient and balanced than that in the device with HTL. Subsequently, the turn-on voltage of the simple device (4.5 V) is lower than that of the one with dedicated HTL (5.0 V). Profiting from the better electronic property, the simple configuration OLED radiates more brightly with a maximum luminance (L_{max}) of 5060 cd/m^2 at 15 V, which is much higher than the one with HTL of 1410 cd/m^2 ; and also, the simple device exhibits much higher efficiencies. Figure 9 shows the current efficiency and external quantum efficiency versus voltage characteristics of the two kinds of devices. The efficiency of the simple device is more than double times than that of the multilayer one in the whole bias range, e.g., 5.7 cd/A Vs 1.7 cd/A of the maximum current efficiency (CE), and 2.3% Vs 1.5% of the external quantum efficiency (EQE). (For details, see Table 2.) These results clearly demonstrated the intrinsic hole-transporting ability of the carbazole-containing lumigen.

Table 2 Electroluminescence performances of DCDPE.^a

HTL	λ_{EL} (nm)	V_{on} (V)	L_{max} (cd/m^2)	CE_{max} (cd/A)	PE_{max} (lm/W)	EQE_{max} (%)
√	512	5.0	1410	1.7	1.7	1.5
×	512	4.5	5060	5.7	3.4	2.3

^a Device structures: with HTL, ITO/NPB(40nm)/DCDPE(20nm)/TPBi (10nm)/Alq3(30nm)/LiF/Al(200nm); without HTL, ITO/DCDPE(60nm)/TPBi(10nm)/Alq3(30nm)/LiF/Al(200nm). Abbreviations: λ_{EL} = EL maximum, V_{on} = turn-on voltage at 1 cd/m^2 , L_{max} = maximum luminance, CE_{max} = maximum current efficiency, PE_{max} = maximum power efficiency, EQE_{max} = maximum external quantum efficiency.

Conclusions

In this paper, a carbazole-containing tetraphenylethene DCDPE is designed and synthesized. Its optical, thermal and optoelectronic properties are investigated. The dye exhibits typical aggregation-induced emission property: being nonluminescent when molecularly dissolved in solutions while intensely emissive in aggregate form. Close inspection of the geometric structure and packing motifs of DCDPE in the crystalline state reveals a loose packing characteristic due to the severe twisted conformation and the absence of strong intermolecular π - π interaction. On the other hand, the multiple weak intermolecular C-H... π hydrogen bonds rigidify the molecular conformation and lock the vibrational and rotational freedom of the four aromatic substituents, accounting for the extremely high solid state quantum yield. The dye crystallizes into strong blue emissive fibres showing optical waveguide effect. The OLED devices using it as both light-emitting and hole-transporting material show superior performances. In a word, both enhanced optical and electronic properties were achieved in DCDPE. The present results demonstrate the promise of the carbazole-containing AIE luminogen as optoelectronic candidates especially for the future laser applications.

Acknowledgements

This work was partially supported by the National Basic Research Program of China (Grant Nos. 51303095, 51021062, 50990061, 51003054, and 2013CB834701), and the Research Grants Council of Hong Kong (HKUST2/CRF/10 and N_HKUST620/11). Y. Liu thanks the support from the Independent Innovation Foundation of Shandong University (2011TB020) and the Promotive Research Fund for Young Scientists of Shandong Province (BS2012CL020).

Notes and references

^a State Key Laboratory of Crystal Materials, Shandong University, Jinan 250100, PR China.

E-mail: liuyangicm@sdu.edu.cn

txt@sdu.edu.cn

^b Department of Chemistry, Institute of Molecular Functional Materials, The Hong Kong University of Science & Technology (HKUST), Clear Water Bay, Kowloon, Hong Kong, China.

E-mail: tangbenz@ust.hk

^c Center for Display Research, HKUST, Kowloon, Hong Kong, China

^d Guangdong Innovative Research Team, SCUT-HKUST Joint Research Laboratory, State Key Laboratory of Luminescent Materials and Devices, South China University of Technology, Guangzhou 510640, China

^e HKUST Shenzhen Research Institute, Nanshan, Shenzhen 518057, China

† Electronic supplementary information (ESI) available: Experimental procedures and characterization data, absorption spectra, TEM images, and CIF file See DOI: 10.1039/x0xx00000x /

- 1 W. Hu, F. Ba, X. Gong, X. Zhan, H. Fu, T. Bjornholm, *Organic Optoelectronics*, Wiley VCH, **2013**.
- 2 K.-T. Wong, Y.-Y. Chien, R.-T. Chen, C.-F. Wang, Y.-T. Lin, H.-H. Chiang, P.-Y. Hsieh, C.-C. Wu, C. H. Chou, Y. O. Su, G.-H. Lee and S.-M. Peng, *J. Am. Chem. Soc.*, **2002**, *124*, 11576.
- 3 (a) Z. Yang, Z. Chi, B. Xu, H. Li, X. Zhang, X. Li, S. Liu, Y. Zhang and J. Xu, *J. Mater. Chem.*, **2010**, *20*, 7352; (b) Z. Jiang, T. Ye, C. Yang, D. Yang, M. Zhu, C. Zhong, J. Qin, and D. Ma, *Chem. Mater.* **2011**, *23*, 771.
- 4 Joseph R. Lakowicz, *Principles of fluorescence spectroscopy*, 3rd ed., Springer, **2006**.
- 5 I. F. Perepichka, D. F. Perepichka, *Handbook of Thiophene-Based Materials: Applications in Organic Electronics and Photonics*, John Wiley & Sons, **2009**.
- 6 Y. Zou, T. Ye, D. Ma, J. Qin and C. Yang, *J. Mater. Chem.*, **2012**, *22*, 23485
- 7 Y. G. Wu, J. Y. Zhang, Z. S. Bo, *Organic Letters* **2007**, *9*, 4435.
- 8 M. Zhu and C. Yang, *Chem. Soc. Rev.*, **2013**, DOI: 10.1039/C3CS35440G
- 9 (a) Z. Zhao, J. W. Y. Lam and B. Z. Tang, *J. Mater. Chem.*, **2012**, *22*, 23726; (b) Y. Liu, S. Chen, J. W. Y. Lam, P. Lu, R. T. K. Kwok, F. Mahtab, H. S. Kwok, and B. Z. Tang, *Chem. Mater.*, **2011**, *23*, 2536; (c) Y. Liu, Y. Lv, X. Zhang, S. Chen, J. W. Y. Lam, P. Lu, R. T. K. Kwok, H. S. Kwok, X. Tao, and B. Z. Tang, *Chem. Asian J.*, **2012**, *7*, 2424; (d) Y. Liu, S. Chen, J. W. Y. Lam, F. Mahtab, H. S. Kwok and B. Z. Tang, *J. Mater. Chem.*, **2012**, *22*, 5184.
- 10 (a) Y. Hong, J. W. Y. Lam, B. Z. Tang, *Chem. Soc. Rev.*, **2011**, *40*, 5361; (b) Y. Liu, Y. Tang, N. N. Barashkov, I. S. Irgibaeva, J. W. Y. Lam, R. Hu, D. Birimzhanova, Y. Yu, and B. Z. Tang, *J. Am. Chem. Soc.*, **2010**, *132*, 13951; (c) Y. Liu, Y. Yu, J. W. Y. Lam, Y. Hong, M. Faisal, W. Yuan, B. Z. Tang, *Chem. Eur. J.*, **2010**, *16*, 8433.
- 11 Y. Hong, J. W. Y. Lam and B. Z. Tang, *Chem. Commun.*, **2009**, 4332.
- 12 Z. Zhao, S. Chen, J. W. Y. Lam, P. Lu, Y. Zhong, K. S. Wong, H. S. Kwok, B. Z. Tang, *Chem. Commun.*, **2010**, *46*, 2221.
- 13 (a) Y. Liu, X. Chen, Y. Lv, S. Chen, J. W. Y. Lam, F. Mahtab, H. S. Kwok, X. Tao, and B. Z. Tang, *Chem. Eur. J.*, **2012**, *18*, 9929; (b) Y. Liu, Y. Lv, H. Xi, X. Zhang, S. Chen, J. W. Y. Lam, R. T. K. Kwok, F. Mahtab, H. S. Kwok, X. Tao and B. Z. Tang, *Chem. Commun.*, **2013**, *49*, 7216.
- 14 K. Naito, A. Miura, *J. Phys. Chem.* **1993**, *97*, 6240.
- 15 R. Kim, S. Lee, K.-H. Kim, Y.-J. Lee, S.-K. Kwon, J.-J. Kim and Y.-H. Kim, *Chem. Commun.*, **2013**, *49*, 4664.